Original Article
Improved speckle contrast optical coherence tomography angiography

Liwei Wang, Yuejie Li, Yilu Li, Kaining Li

Institute of Biomedical Engineering, Chinese Academy of Medical Sciences and Peking Union Medical College, Tianjin 300192, China

Abstract: Optical coherence tomography (OCT) is becoming a clinically useful and important imaging technique due to its ability to provide high-resolution structural imaging *in vivo*. Optical coherence tomography angiography (OCTA) can visualize vasculature imaging of biological tissues. With the advent of Fourier-domain OCT, numerous OCTA techniques have been developed to detect the microvasculature *in vivo*. The macular region of the fundus is separated into retinal and choroid regions by segmentation algorithm in the data processing, a false blood flow signal is generated due to bulk motion when vasculature imaging was segmented in the retinal regions. However, the most recent OCT angiographic approaches are sensitive to bulk motion noise. To overcome this limitation, we proposed an improved speckle contrast optical coherence tomography angiography (ISC-OCTA) algorithm to image vasculature network *in vivo*. The improved speckle contrast image was acquired by the improved speckle contrast algorithm for *N* consecutive frames of the same location, and the vasculature of the tissue was generated by masking the averaged image with the improved speckle contrast image. ISC-OCTA was tested on *in vivo* images of a phantom mouse ear and a human macula. Compared to the recently reported algorithms, we found that ISC-OCTA can distinguish the dynamic information of blood flow from static tissue and visualize capillary vessels. Especially when the segmentation data generates false information, the ISC-OCTA algorithm has a significant effect on the suppression of the line noise. ISC-OCTA can provide clear visualization of vessels as other algorithms and may be useful in the diagnosis of ophthalmic diseases.

Keywords: Optical coherence tomography, optical coherence tomography angiography, microcirculation, speckle contrast, blood vessels

Introduction

It is well-known that microcirculation is blood circulation between arterioles and venules. Microcirculation dysfunction may lead to tissue dysfunction, which is a major cause of many diseases. Changes in structure and function of microcirculation may be clinically related to various pathological conditions. Therefore, it is feasible to detect the early features of microcirculation for diagnosis of clinical diseases at an early stage.

Optical coherence tomography [1] is an optical modality for high-resolution imaging of biological tissue. The key advantages of using optical coherence tomography (OCT) as a detection technique include high resolution, high speed, high sensitivity; moreover, it is non-invasive *in*

vivo, and it has mutually independent horizontal and axial resolution. With the recent development of light sources and detection techniques, the applications of OCT are diverse, such as dermatology [2, 3], gastroenterology [4], cardiology [5], and neurology [6]. Moreover, the goals of the OCT system were to switch from structural imaging to functional imaging, which could stimulate development in optical coherence tomography angiography (OCTA) algorithms by utilizing different components of OCT signals, including phase signals, intensity signals and complex signals [7, 8].

It is obvious that OCTA has become an important technique for angiography due to its high resolution of capillary-vessel microcirculation in tissue [7, 8]. Numerous OCT angiographies have been successfully developed to image

blood flow in human, such as B-M mode scanning (including speckle variance [9], phase variance [10], correlation mapping [11], split-spectrum amplitude-decorrelation [12], and optical microangiography [13-16]) and repeated A-line scanning mode (including Doppler OCT [17], Doppler variance [18], and Doppler optical micro-angiography [19]).

Barton and Stromski [20] first proposed the speckle concept by use of time-domain OCT. With the development of FD-OCT, Marriampillai et al. [21] proposed speckle variance (SV) OCTA by calculating the speckle variance of the OCT structural images:

$$I_{SV} = \frac{1}{N} \sum_{i=1}^{N} \left(I_i - \frac{1}{N} \sum_{i=1}^{N} I_i \right)^2 \tag{1}$$

where I_i is an intensity value at i'th B-scan structural frame in the slow scan direction, N is the number of B-scans.

Blatter et al. proposed a Fourier domain mode locked (FDML) [22] algorithm by calculating the squared intensity difference between consecutive frames:

$$I_{Flow} = [I_i - I_{i+1}]^2 \tag{2}$$

where I_i is an intensity value at i'th B-scan structural frame in the slow scan direction.

Wang et al. proposed an optical microangiography (OMAG) [13-15] algorithm that utilized the subtraction between repeated frames to calculate the complex differentiation. OMAG may provide the best visual result of retinal microvascular networks [7]:

$$F = \frac{1}{N-1} \sum_{i=0}^{N-1} |C_{i+1} - C_i| \tag{3}$$

where i is the index for the repeated B-scans at each position, C is the motion corrected complex OCT signal and N is the number repeated in each step.

Huang et al. [16] also proposed an algorithm by performing intensity subtraction (ISUB) between repeated B-frames based on the OMAG algorithm:

$$I_{Flow} = \frac{1}{N-1} \sum_{i=0}^{N-1} |I_{i+1} - I_i| \tag{4}$$

where $I_i = |C_i|$ is the amplitude of the complex signal at i'th B-scan structural frame in the slow scan direction, and N is the number of B-scans. This algorithm is a much more practical solution for OMAG [16].

Laser speckle contrast imaging (LSCI) is a wide-field two-dimensional imaging technique that can quickly acquire the distribution of the dynamic blood flow within tissue beds *in vivo* [23]. LSCI was recently used in visualization of blood flow for applications in dermatology [24] and neurosurgery [25]. In this study, we extended the LSCI method to the OCTA field and proposed an improved speckle contrast optical coherence tomography angiography (ISC-OCTA) algorithm. We performed experiments on flow phantoms and animal models to verify the algorithm. Finally, images of the human ocular fundus vasculature were collected using ISC-OCTA technique as well.

Materials and methods

System setup

In this study, a customized Fourier domain OCT (FD-OCT) system for imaging was adopted. The FD-OCT system was equipped with a broadband super luminescent diode at 840 nm (Inphenix Inc, Livermore, CA, USA) as the light source, has a bandwidth range of 50 nm, a measured axial resolution of ~ 5 μm (full-width half-maximum amplitude profile) and an imaging range of 2 mm in tissue. The light output power of the sample arm is below 750 μW. The system spectrum was collected by the line camera at a rate of 70K lines/s. Along the X-scanning direction, 256 A-lines were captured in a B-scan at a frame rate of 200 frames/s. In the Y-scanning direction, 2048 B-Scans were acquired at 256 continuous transversal locations within ~10 s. 8 consecutive B-Scan frames were acquired at each location to evaluate the relative performance of different OCT angiographic algorithms.

ISC-OCTA processing technique

OCT structural frames were obtained after applying fast Fourier transformation (FFT). N consecutive frames of the same location were repeatedly scanned and matched; the matched frames were averaged to enhance the intensity of blood flow signals, and the improved speckle

contrast image was used to obtain the information of the dynamic blood flow. Finally, the vasculature of tissue was generated by masking the averaged image with the improved speckle contrast image. We found that ISC-OCTA can exclude the information of static tissue while preserving the information of the dynamic blood flow.

Image matching: N consecutive B-Scan frames were repeatedly captured at each transversal location, and M transversal locations were acquired. During the image acquisition process, the target movements can easily cause motion artifacts [26, 27] between B-scans, such as respiration or pulsation. Motion artifacts will lead to the loss of data continuity, especially for the detection of blood flow information, and it was difficult to distinguish the static tissue from the dynamic tissue during post-processing. Therefore, to compensate for motion artifacts due to respiration or pulsation, N consecutive structural frames were aligned by means of a module matching algorithm before vascular mapping.

Image averaging: Background noise is random between B-scan frames. To suppress noise due to bulk motion and background noise, N matched frames were averaged; the intensity of static tissue remain unchanged, and the blood flow signals were enhanced, as described in Equation (5).

$$I_s(x, y_j, z) = \frac{1}{N} \sum_{i=1}^{N} (x, y_i, z) \qquad (5)$$

where $I(x, y_i, z) = | FFT[I(x, y_i, k)] |$ is an intensity value at i'th B-scan structural frame in the slow scan direction, k is the wavenumber, and x, y and z are horizontal, axial and depth indices of the B-scan frames, respectively. N consecutive frames are averaged to increase signal sensitivity in the flow region. I_s is the average image, which contains the information of static tissue and dynamic blood flow.

Improved speckle contrast imaging: The speckle contrast (SC) [28, 29] is defined as the ratio of the standard deviation to the mean intensity, as described in Equation (6).

$$K = \frac{\delta}{\bar{I}} \qquad (6)$$

where δ is the standard deviation of the speckle intensity, κ is the speckle contrast, and $\bar{I}$ is mean of the image intensity. Motion artifacts are generated during image acquisition. The shorter the image acquisition time interval, the smaller the motion artifact is; however, there is still slight motion between two consecutive frames after image matching. The dispersion of data δ is increased during the average operation for the motion artifact; thus, we proposed an improved speckle contrast (ISC) algorithm described by Equation (7). The improved speckle contrast image K_S was acquired by performing speckle contrast analysis on two consecutive frames.

$$K_s(x, y_j, z) = \frac{1}{N-1} \sum_{i=1}^{N-1} \frac{| I(x, y_{i+1}, z) \bar{} I(x, y_i, z) |}{I(x, y_{i+1}, z) + I(x, y_i, z)} \qquad (7)$$

Image marking: Improved speckle contrast image K_S contains static tissue and dynamic tissue information. The value of K_S in static tissue is smaller than the dynamic tissue; thus, the final blood flow image (I_{flow}) was generated by masking the average image with the improved speckle contrast image. I_{flow} is described in Equation (8). This approach reduced the background noise, eliminated the high intensity value of the static tissue signal, and enhanced the blood flow signal. Using the same approach for M locations the blood flow image was finally acquired.

$$I_{flow}(x, y_j, z) = I_S(x, y_j, z) * K_S(x, y_j, z) \qquad (8)$$

Statistical analysis

We used Statistical Product and Service Solutions (SPSS) 19.0 software (IBM, Armonk, NY, USA) for statistical analysis. Measurement data of experiments was represented as the mean ± standard deviation. The paired t-test was used for comparing differences between the two groups. $P < 0.05$ was considered statistically significant.

Results

Phantom imaging

First, we performed flow phantom experiments to verify the ISC-OCTA algorithm. A transparent tube (inner diameter of 300 μm and external diameter of 500 μm) was placed in water, and a
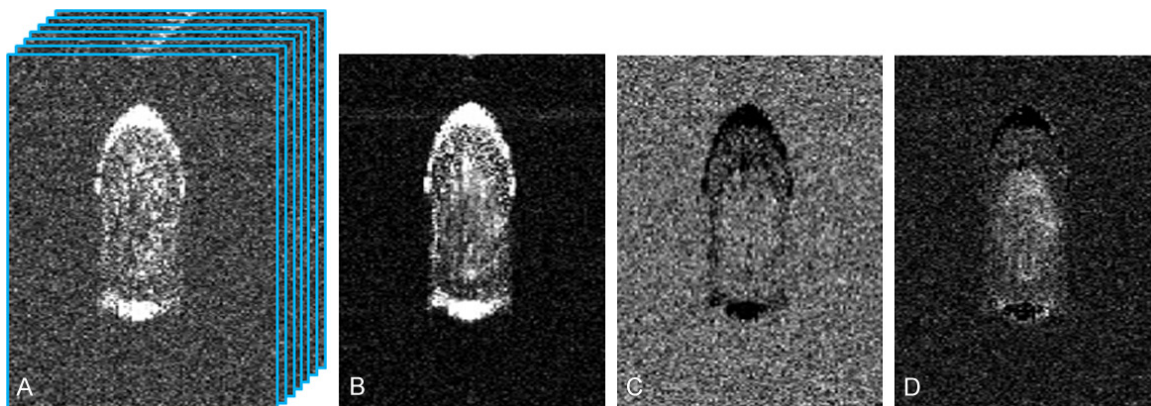
Figure 1. ISC-OCTA Phantom imaging. A. 8 consecutive B-Scan frames were repeatedly captured at each transversal location, and consecutive structural frames were aligned by means of a module matching algorithm. B. 8 matched frames were averaged, the intensity of static tissue remains unchanged, and the blood flow signals were enhanced. C. The improved speckle contrast image was acquired by performing speckle contrast analysis on two consecutive frames. D. ISC-OCTA flow image of phantom was generated by masking the average image with the improved speckle contrast image.
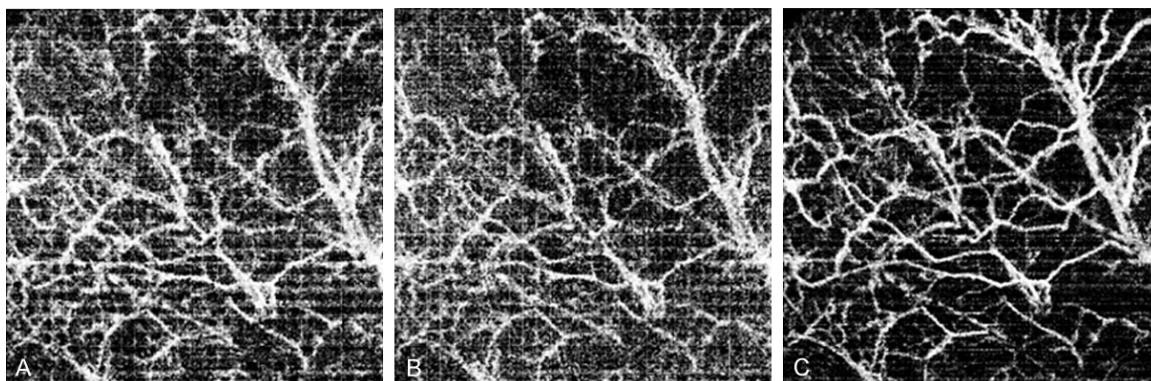

Figure 2. Comparison between three intensity angiography algorithms: SC, ISC, and ISC-OCTA, 3D OCT volume data consisted of a field of view of 5.0 mm × 5.0 mm in the right eye of a mouse. A. *En face* maximum reflectance intensity projection of SC microvasculature was acquired by Equation 2. B. *En face* maximum reflectance intensity projection of ISC microvasculature was acquired by Equation 3. C. *En face* maximum reflectance intensity projection of ISC-OCTA microvasculature was acquired by Equation 4.

mixture of rabbit blood infused with heparin (anticoagulant) [30] was pumped through the tube at rate of 2 mL/h to mimic blood flow in the blood vessel by a syringe pump (Howkmed Medical Instrument, Inc, Shenzhen, CHN).

Consecutive structural frames were acquired after applying FFT. To reduce motion noise, each pair of consecutive frames were aligned using a module matching algorithm before vascular mapping; then the matched frames (**Figure 1A**) were averaged to generate the average image (**Figure 1B**). The signals from the water were invisible surrounding the transparent tube, but the stronger reflection signals

at the outer layer of the tube were still observed. The improved speckle contrast was performed on the matched frames to generate the improved speckle contrast image (**Figure 1C**), and the signals of the tube wall were basically eliminated. The final blood flow image (**Figure 1D**) was generated by masking the averaged image with the improved speckle contrast image; the intensity of the pipe was obviously weakened, the stronger reflected signal on the pipe wall was basically eliminated, the noise had been significantly suppressed, and we could see the fluid region clearly. The ISC-OCTA algorithm is valid for phantom.
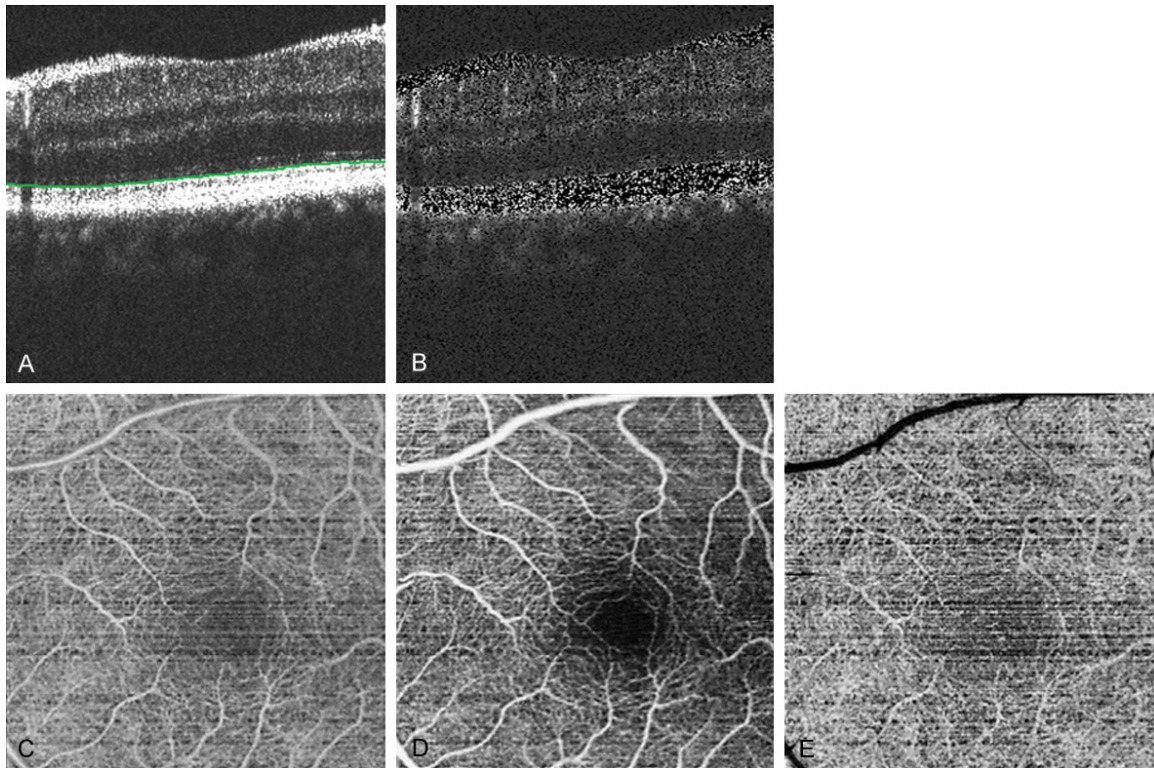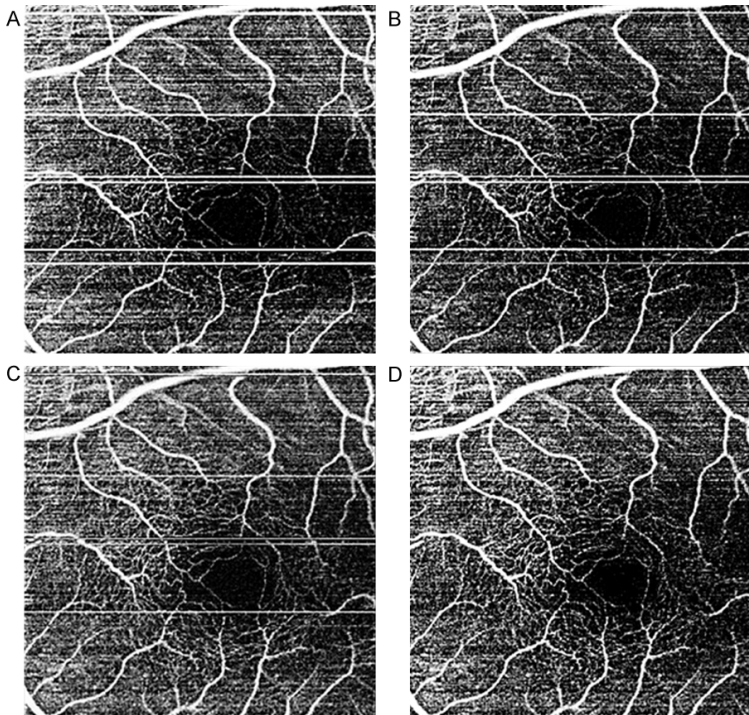
Figure 3. Examples of ISC-OCTA angiograms of macula from healthy human subjects, *in vivo* 3D OCT volume data of the macula consisted of a field of view of 3.0 mm × 3.0 mm. A. Cross-sectional OCT structural image through the foveal center with structure information. B. Cross-sectional OCT blood flow image through the foveal center with flow information. C. *En face* maximum reflectance intensity projection image of ISC-OCTA microvascular flow from the whole ocular fundus; D. *En face* maximum reflectance intensity projection image of ISC-OCTA microvascular flow above IS/OS layer; E. *En face* maximum reflectance intensity projection image of ISC-OCTA microvascular flow following layer.

Mouse ear angiography

All animal procedures were conducted following the protocol approved by the Institutional Laboratory Animal Ethics Committee and the Institutional Animal Care and Use Committee, Peking Union Medical College, People's Republic of China. All animal experiments were performed in compliance with the Guiding Principles for the Care and Use of Laboratory Animals, Peking Union Medical College, People's Republic of China. Animals were housed in cages with free access to food and water.

We performed animal experiments to contrast and analyze the imaging results. A 9-week-old female nude mouse was anesthetized by injecting 250 microliters ammonium 4% hydrogen hydrate before imaging and was put on the surface of the platform in order to reduce the motion effect. The nude mouse's right ear was fixed to the surface of the platform by double-sided tape. We performed animal experiments and made comparisons among three speckle contrast angiography algorithms. 3D OCT volume data consisted of a field of view of 5.0 mm × 5.0 mm. SC microvasculature (**Figure 2A**) was acquired by Equation 2 can visualize the vasculature. **Figure 2A** shows the microvasculature of the ear tissue of the mouse clearly, but the noise of the image was relatively strong due to the false blood flow signal generated by the bulk motion, and the line noise was obvious. **Figure 2B** is ISC microvasculature (by Equation 3). The noise of the image, especially the noise of the lines, was significantly suppressed using improved speckle contrast technique, and the image showed better quality than the SC image; **Figure 2C** is ISC-OCTA microvasculature (by Equation 4). By using the ISC image and the mean image to multiply, the background noise was further reduced and the line noise was also suppressed. The result showed that the ISC-OCTA image has a higher signal-to-noise

Figure 4. Performance comparison between four intensity angiography algorithms for blood flow signal data with false segmentation: SV, FDML, ISUB and ISC-OCTA, *in vivo* 3D OCT volume data of the macula consisted of a field of view of 3.0 mm × 3.0 mm. A-D. *En face* maximum reflectance intensity projection images of the blood vessel network visualized by SV, FDML, ISUB and ISC-OCTA algorithms.
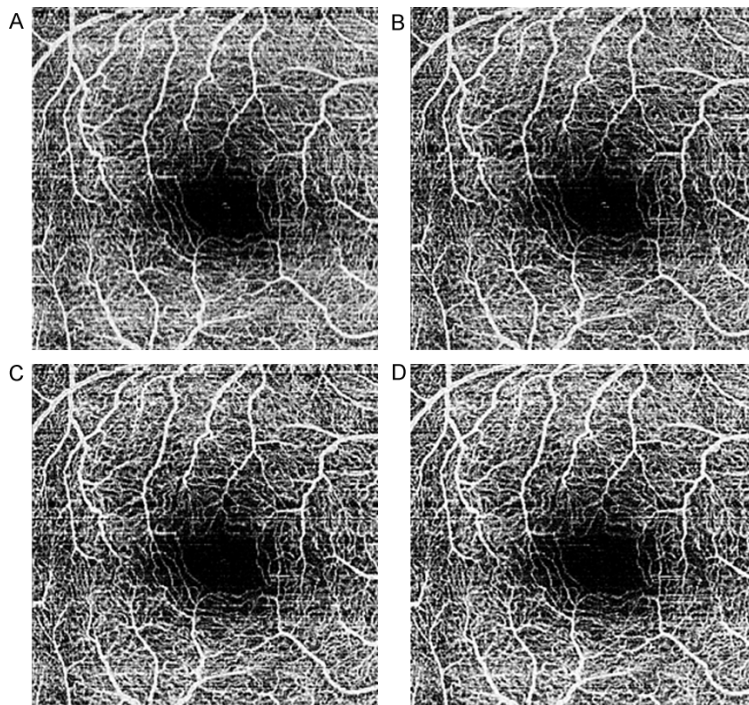
Figure 5. Performance comparison between four intensity angiography images for healthy human subjects, *in vivo* 3D OCT volume data of the macula

consisted of a field of view of 3.0 mm × 3.0 mm. A-D. *En face* maximum reflectance intensity projection images of the blood vessel network in normal human macular visualized by SV, FDML, ISUB and ISC-OCTA algorithms.

ratio and has the best visualization effect.

Macular angiography

All procedures performed in studies involving human participants were in accordance with the ethical standards of the institutional ethics committee and with the 1964 Helsinki Declaration and its later amendments or comparable ethical standards.

Finally, we captured the image of the vasculature in the human macula of five normal male volunteers with a view of 3.0 mm × 3.0 mm. As shown in **Figure 3A**, we can see the retinal IS/OS layer (green line) clearly in the cross-sectional structural image. Furthermore, we obtained blood flow images by using the ISC-OCTA algorithm (**Figure 3B**). The static tissue signal was effectively restrained; the dynamic blood flow signal was relatively enhanced. We can calculate different depths of the retinal image. **Figure 3C** is the *enface* blood flow image of the whole macula, **Figure 3D** is the above IS/OS layer, and **Figure 3E** is the following layer. The ISC-OCTA image was similar to images from previously reported angiography techniques [7]. The flow pixels formed a continuous retinal vessels network. There were no retinal vessels within the foveal avascular zone (**Figure 3D**), which agrees with known anatomy.
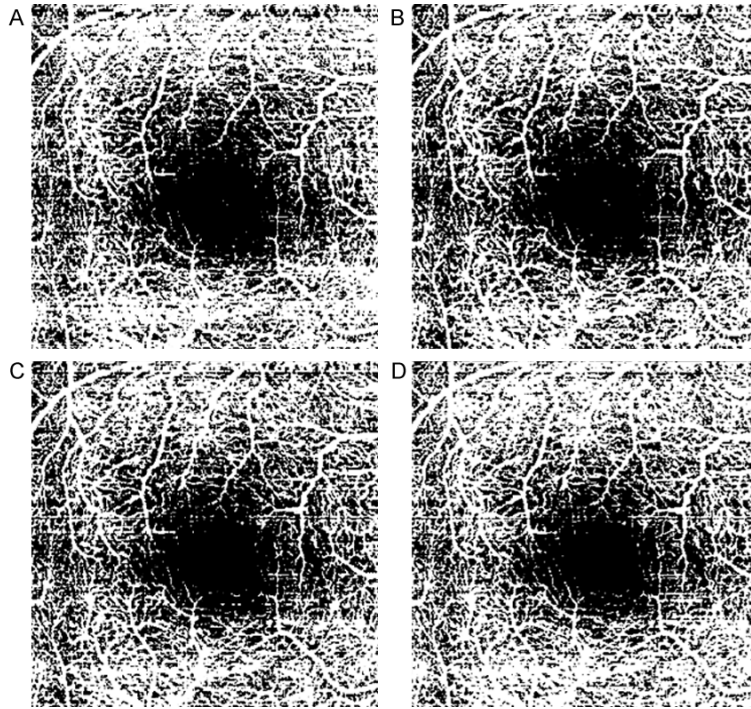
Figure 6. A-D. Binarized images for SV, FDML, ISUB and ISC-OCTA images.
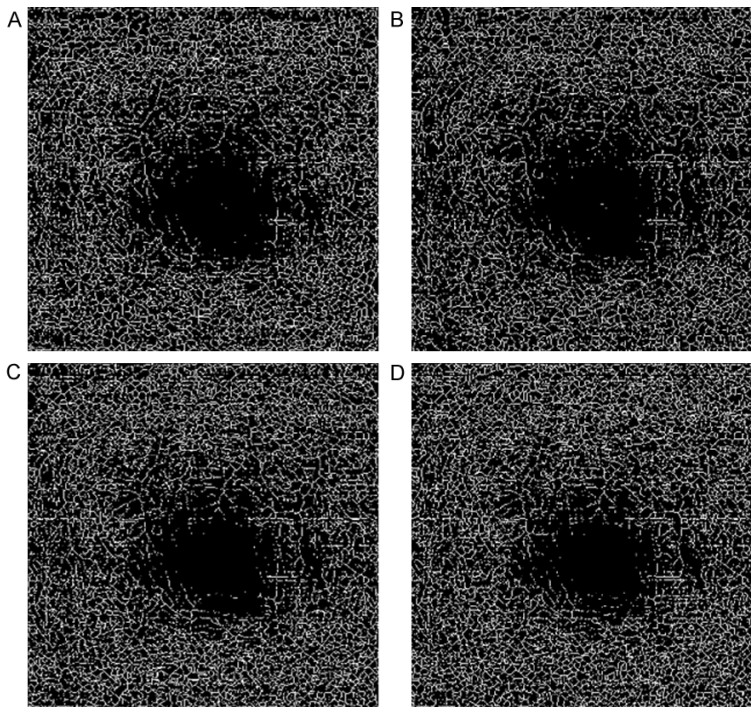

Figure 7. A-D. Skeletonized images for SV, FDML, ISUB and ISC-OCTA images.

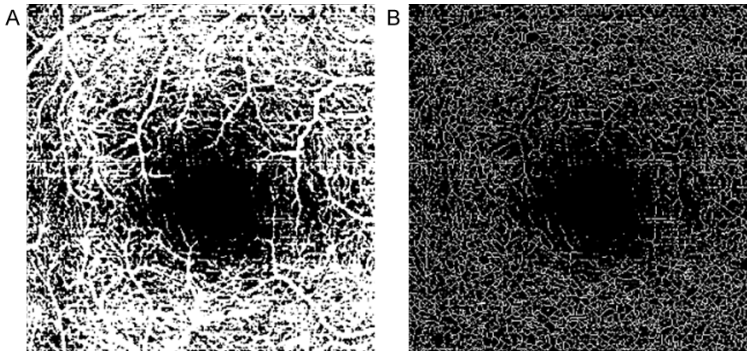*Comparison between four intensity angiography algorithms: SV, FDML, ISUB, and ISC-OCTA*

To assess the performance of the algorithm, we compared it with other algorithms. A general literature review [7] is provided on the recent progress of OCT angiography algorithms, speckle variance, FDML and intensity subtraction algorithms. We captured the structural image of the vasculature from the same retina of human subjects with a view of 3.0 mm × 3.0 mm.

Comparison on visualization

In the process of data processing, image misalignment may generate false information in blood flow image data due to motion artifact correction and image segmentation. The false information in the two-dimensional blood flow image will cause line noises in the three-dimensional blood flow images, which seriously affects the quality of the *en-face* image. After retinal image segmentation, due to bulk motion and segmentation errors, a false blood flow signal is generated during vascular imaging. We use the same set of data with false blood flow signals for processing, and the results are shown in **Figure 4**. We used Equations 1, 2, 4, and 8 to process and obtain the SV (**Figure 4A**), FDML (**Figure 4B**), ISUB (**Figure 4C**) and ISC-OCTA (**Figure 4D**) images. The difference between the four algorithms can be appreciated by visual inspection of the images. SV and FDML images are calculated by using the standard deviation and the square of the adjacent image difference, which have the same display effect, and the line noise is relatively obvious. The ISUB image showed better quality than the SV and FDML images, and the line noise was also suppressed. Compared with other algorithms, the results show that the ISC-OCTA algorithm has the best performance for line noise suppression.

Figure 8. A, B. Binarized and skeletonized images for mean image.

re expressed as the mean ± standard deviation. The results showed that the ISC-OCTA algorithm had significantly better SNR relative to the SV (P = 0.027), FDML (P = 0.036) and ISUB (P = 0.027). The difference was statistically significant (P < 0.05). The signal-to-noise ratio of the ISC-OCTA algorithm is improved by 124% compared to the SV algorithm.

Comparison of connectivity, contrast and signal-to-noise ratio

To assess the performance of the algorithm, we converted projection images obtained by four different angiography algorithms (**Figure 5**) of five eyes of the five participants. The results show that realized fundus retinal blood flow images can be obtained by all four algorithms: the blood flow images have continuous retinal vessels network and no retinal vessels within the foveal avascular zone, consistent with the results reported in the relevant literature (Ref [7, 12]). **Figure 6** shows binarized images, and **Figure 7** shows skeletonized images.

Vessel connectivity, image contrast, and signal-to-noise ratio (SNR) can be used to evaluate the performance of the blood flow imaging. We obtained the binary images with a morphological operation. The vascular network was made of 1-pixel wide lines with a skeletonizing morphological operation. We averaged the blood flow images of all the algorithms as the mean image, binarized the mean image to generate a skeleton image as a mask image $S(x, y)$ (**Figure 8**). To calculate vessel connectivity, image contrast, and SNR for the blood flow image, we defined relevant signal and noise regions by using the binary and skeletonized image of blood flow; the skeletonized vascular network are the relevant signal regions, and the regions outside the branched vessels are the noise regions. Then, we used the following formula in Equations 9-117. Performance comparison was analyzed on the OCT macular angiograms of five eyes of five participants (**Table 1**). We compared the four algorithms based on paired t-tests, and the data we-

$$Connectivity = std\,[I(x,y)\mid s(x,y) = 1] \qquad (9)$$

$$Contrast = \frac{Mean\,[I(x,y)\mid s(x,y) = 1]}{Std\,[I(x,y)\mid s(x,y) = 1]} \qquad (10)$$

$$SNR = \frac{Mean\,[I(x,y)\mid s(x,y) = 1]}{Std\,[noise]} \qquad (11)$$

En-face blood flow images of four algorithms can provide good blood flow information, ISC-OCTA image has not any retinal vessels in the foveal avascular zone [12] and the best performance.

Discussion

The effectiveness of the ISC-OCTA algorithm was verified by the phantom experiment. **Figure 1** shows that the ISC-OCTA algorithm is valid for phantom; the intensity of the pipe was obviously weakened in the final blood flow image (**Figure 1D**), the stronger reflected signal on the pipe wall was basically eliminated, the noise had been significantly suppressed, and the fluid region can be seen clearly. Through animal experiments, the ISC-OCTA algorithm has a significant effect on the improvement of signal-to-noise ratio compared to SC and ISC algorithms. The ISC-OCTA algorithm (**Figure 2**) has the best signal-to-noise ratio in the animal experiment. Compared with performing subtraction between consecutive B-scans, the average process can preserve the blood flow information effectively. Because the signals of dynamic blood flow in the overlapped area are also relatively suppressed, the dynamic blood flow information may be lost at the subtraction of consecutive frames. Through the averaging process the static tissue signals remain unchanged, dynamic blood flow signals are enhanced, and back-

Table 1. Performance comparisons of four algorithms blood flow images

	SV	FDML	ISUB	ISC-OCTA
Connectivity	0.2742 ± 0.04742	0.2528 ± 0.05277	0.2128 ± 0.02767	0.1788 ± 0.01426
Contrast	2.0215 ± 0.42452	2.2796 ± 0.46882	1.7181 ± 0.93371	2.5545 ± 0.60089
SNR	2.4193 ± 1.62217	2.5958 ± 1.73418	2.7105 ± 1.41906	5.4269 ± 0.6413
Improvement of SNR	NA	7.3%	12%	124.3%

Statistical analysis is based on 5 eyes of 5 normal human subjects.
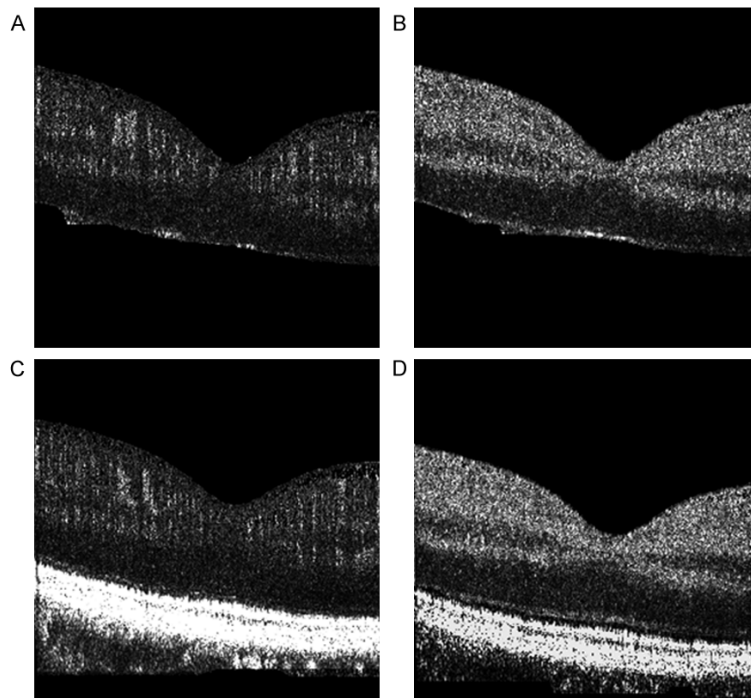
Figure 9. Cross-sectional OCT blood flow image. A. Real blood flow image cross-sectional OCT blood flow image. B. The false blood flow image is caused by image motion artifacts. C. The false blood flow image is caused by incorrect image segmentation. D. The false blood flow image is caused by both motion artifacts and incorrect segmentation.

flow image, **Figure 9B-D** are the false blood flow images, the false blood flow images are mainly caused by image motion artifacts (**Figure 9B**) and incorrect image segmentation (**Figure 9C**), **Figure 9D** is the result of both. Subtraction can't eliminate the line noise which caused by incorrect image segmentation, but the ISC-OCTA algorithm adopts the division operation, as long as there are two adjacent images segment correctly in the N continuous images collected at the same position, it can ensure that the intensity of other layers is invalid when visualize images in different layers, so, the noise can be significantly suppressed. The ISC-OCTA algorithm can provide clear visualization of vessels (**Figure 5**) in the human ocular fundus circulations, as previously reported in angiography algorithms [13, 21, 22]. **Table 1** shows that the ISC-OCTA image significantly improved both SNR and connectivity when compared to others.

The ISC-OCTA algorithm has several potential advantages. One advantage is that ISC-OCTA has the same advantage of angiography based on intensity. Another potential advantage of ISC-OCTA is the possibility of quantifying blood flow velocity. Recently, laser speckle imaging technique has been developed for angiography [31, 32]. Laser speckle imaging has been used to noninvasively monitor blood flow in the retina [33], brain [34], and skin [35]. The motion of red blood cells causes intensity changes that can be analyzed with temporal, spatial, or combined spatiotemporal speckle contrast algorithms. The speckle contrast value is propor-

ground random scattered light noise was reduced. **Figure 4** shows that ISC-OCTA has the best performance for line noise suppression and delivered significant anti-interference when compared to other algorithms. In the data processing of other algorithms, in which the subtraction operation and the mean operation are used, the false two-dimensional blood flow information is not obviously suppressed. However, the ISC-OCTA algorithm uses adjacent two-dimensional images for blood flow imaging (the operation is performed by using Equation 7), and includes a division operation, which effectively reduces the difference between the false signal and the real signal so that the line noise is suppressed. **Figure 9A** is the real blood

tional to the blood flow velocity. Thus, in OCTA results the speckle contrast value may be a function of the flow velocity. To accurately measure blood flow velocity, we will conduct *in vitro* flow phantom experiments to calibrate the speed.

The ISC-OCTA algorithm has some limitations; one limitation is that it cannot completely eliminate the impact of motion artifacts. Although the ISC-OCTA algorithm can suppress the influence of bulk motion noise it cannot eliminate the bulk motion noise, so image registration processing is still required. In this paper, we compensated X-Z motion by the use of a module matching algorithm. This algorithm could reduce the effect of motion artifacts in the X-Z dimensions. Due to processing time requirements, we made no attempt to compensate for the Y direction. Motion compensation can either be done with an active motion tracking system [36] or post-processing. This could potentially be reduced by the use of 3D registration algorithms [37]. Another limitation is data processing time; we can attempt to reduce the number of repeated B-scans or use cameras with higher acquisition speeds.

Conclusion

In summary, we exploited an improved speckle contrast angiography, which used the improved speckle contrast blood flow image to mark the average image and eliminated static artifacts while preserving the vessel structures. This approach was validated by the simulation and animal experiments. The result showed that ISC-OCTA can acquire clear ocular fundus microvascular images in *in vivo* experiments and may be useful in the diagnosis of ophthalmic diseases.

Acknowledgements

Disclosure of conflict of interest

None.

Address correspondence to: Yuejie Li, Institute of Biomedical Engineering, Chinese Academy of Medical Sciences and Peking Union Medical College, Tianjin 300192, China. E-mail: liyjbme@163.com

References

[1] Huang D, Swanson EA, Lin CP, Schuman JS, Stinson WG, Chang W, Hee MR, Flotte T, Gregory K, Puliafito CA, Fujimoto JG. Optical coherence tomography. Science 1991; 254: 1178-1181.

[2] Ulrich M, Themstrup L, De CN, Manfredi M, Grana C, Ciardo S, Kästle R, Holmes J, Whitehead R, Jemec GB, Pellacani G, Welzel J. Dynamic optical coherence tomography in dermatology. Dermatology (Basel) 2016; 232: 298-311.

[3] Baran U, Li Y, Choi WJ, Kalkan G, Wang RK. High resolution imaging of acne lesion development and scarring in human facial skin using OCT-based microangiography. Lasers Surg Med 2015; 47: 231-238.

[4] Zagaynova E, Gladkova N, Shakhova N, Gelikonov G, Gelikonov V. Endoscopic OCT with forward-looking probe: clinical studies in urology and gastroenterology. J Biophotonics 2008; 1: 114-128.

[5] Bezerra HG, Costa MA, Guagliumi G, Rollins AM, Simon DI. Intracoronary optical coherence tomography: a comprehensive review: clinical and research applications. J Am Coll Cardiol Intv 2009; 2: 1035-1046.

[6] Dziennis S, Qin J, Shi L, Wang RK. Macro-to-micro cortical vascular imaging underlies regional differences in ischemic brain. Sci Rep 2015; 5: 10051.

[7] Chen CL, Wang RK. Optical coherence tomography based angiography. J Biomed Opt 2017; 8: 1056-1082.

[8] Gao SS, Jia Y, Zhang M, Su JP, Liu G, Hwang TS, Bailey ST, Huang D. Optical coherence tomography angiography. Invest Ophthalmol Vis Sci 2016; 57: 27-36.

[9] Mammo Z, Balaratnasingam C, Yu P, Xu J, Heisler M, Mackenzie P, Merkur A, Kirker A, Albiani D, Freund KB, Sarunic MV, Yu DY. Quantitative noninvasive angiography of the fovea centralis using speckle variance optical coherence tomography. Invest Ophthalmol Vis Sci 2015; 56: 5074-5086.

[10] Kim DY, Fingler J, Werner JS, Schwartz DM, Fraser SE, Zawadzki RJ. *In vivo* volumetric imaging of human retinal circulation with phase-variance optical coherence tomography. Biomed Opt Express 2011; 2: 1504-1513.

[11] Liew YM, McLaughlin RA, Gong P, Wood FM, Sampson DD. "In vivo assessment of human burn scars through automated quantification of vascularity using optical coherence tomography". J Biomed Opt 2013; 18: 061213.

[12] Jia Y, Tan O, Tokayer J, Potsaid B, Wang Y, Liu JJ, Kraus MF, Subhash H, Fujimoto JG, Hornegger J, Huang D. Split-spectrum amplitude-decorrelation angiography with optical coher-

ence tomography. Opt Express 2012; 20: 4710-4725.

[13] An L, Qin J, Wang RK. Ultrahigh sensitive optical microangiography for *in vivo* imaging of microcirculations within human skin tissue beds. Opt Express 2010; 18: 8220-8228.

[14] Wang RK. Optical microangiography: a label free 3D imaging technology to visualize and quantify blood circulations within tissue beds *in vivo*. IEEE J Sel Top Quantum Electron 2010; 16: 545-554.

[15] Wang RK, An L, Francis P, Wilson DJ. Depth-resolved imaging of capillary networks in retina and choroid using ultrahigh sensitive optical microangiography. Opt Lett 2010; 35: 1467-1469.

[16] Huang Y, Zhang Q, Thorell MR, An L, Durbin MK, Laron M, Sharma U, Gregori G, Rosenfeld PJ, Wang RK. Swept-source OCT angiography of the retinal vasculature using intensity differentiation-based optical microangiography algorithms. Ophthalmic Surg Lasers Imaging Retina 2014; 45: 382-389.

[17] Zotter S, Pircher M, Torzicky T, Bonesi M, Götzinger E, Leitgeb RA, Hitzenberger CK. Visualization of microvasculature by dual-beam phase resolved Doppler optical coherence tomography. Opt Express 2011; 19: 1217-1227.

[18] Yu L, Chen Z. Doppler variance imaging for three-dimensional retina and choroid angiography. J Biomed Opt 2010; 15: 016029.

[19] Wang RK, An L. Doppler optical micro-angiography for volumetric imaging of vascular perfusion *in vivo*. Opt Express 2009; 17: 8926-8940.

[20] Barton JK, Stromski S. Flow measurement without phase information in optical coherence tomography images. Opt Express 2005; 13: 5234-5239.

[21] Mariampillai A, Standish BA, Moriyama EH, Khurana M, Munce NR, Leung MKK, Jiang J, Cable A, Wilson BC, Vitkin IA, Yang aVXD. Speckle variance detection of microvasculature using swept-source optical coherence tomography. Opt Lett 2008; 33: 1530-1532.

[22] Blatter C, Klein T, Grajciar B, Schmoll T, Wieser W, Andre R, Huber R, Leitgeb RA. Ultrahigh-speed non-invasive widefield angiography. J Biomed Opt 2012; 17: 070505.

[23] Regan C, Hayakawa C, Choi B. Momentum transfer monte carlo for the simulation of laser speckle imaging and its application in the skin. Biomed Opt Express 2017; 8: 5708-5723.

[24] Yang B, Yang O, Guzman J, Nguyen P, Crouzet C, Osann KE, Kelly KM, Nelson JS, Choi B. Intraoperative, real-time monitoring of blood flow dynamics associated with laser surgery of port wine stain birthmarks. Lasers Surg Med 2015; 47: 469-475.

[25] Richards LM, Shame Kazmi SS, Olin KE, Waldron JS, Fox DJ, Dunn AK. Intraoperative multi-exposure speckle imaging of cerebral blood flow. J Cereb Blood Flow Metab 2017; 37: 3097-3109.

[26] Huang D, Jia Y, Gao SS, Lumbroso B, Rispoli M. Optical coherence tomography angiography using the optovue device. Dev Ophthalmol 2016; 56: 6-12.

[27] Rosenfeld PJ, Durbin MK, Roisman L, Zheng F, Miller A, Robbins G, Schaal KB, Gregori G. ZEISS angioplex spectral domain optical coherence tomography angiography: technical aspects. Dev Ophthalmol 2016; 56: 18-29.

[28] Boas DA, Dunn AK. Laser speckle contrast imaging in biomedical optics. J Biomed Opt 2010; 15: 011109.

[29] Fredriksson I, Larsson M. Vessel packaging effect in laser speckle contrast imaging and laser Doppler imaging. J Biomed Opt 2017; 22: 1-7.

[30] Kim J, Oh J, Choi B. Magnetomotive laser speckle imaging. J Biomed Opt 2010; 15: 011110.

[31] Briers JD, Webster S. Quasi real-time digital version of single-exposure speckle photography for full-field monitoring of velocity or flow fields. Opt Commun 1995; 116: 36-42.

[32] Briers JD, Richards G, He XW. Capillary blood flow monitoring using laser speckle contrast analysis (LASCA). J Biomed Opt 1999; 4: 164-75.

[33] Hirao M, Oku H, Goto W, Sugiyama T, Kobayashi T, Ikeda T. Effects of adenosine on optic nerve head circulation in rabbits. Exp Eye Res 2004; 79: 729-735.

[34] Dunn A, Devor A, Dale A, Boas D. Spatial extent of oxygen metabolism and hemodynamic changes during functional activation of the rat somatosensory cortex. Neuroimage 2005; 27: 279-290.

[35] Choi B, Ramirez-San-Juan JC, Lotfi J, Nelson JS. Linear response range characterization and *in vivo* application of laser speckle imaging of blood flow dynamics. J Biomed Opt 2006; 11: 041129.

[36] Zhang Q, Huang Y, Zhang T, Kubach S, An L, Laron M, Sharma U, Wang RK. Wide-field imaging of retinal vasculature using optical coherence tomography-based microangiography provided by motion tracking. J Biomed Opt 2015; 20: 066008.

[37] Kraus MF, Potsaid B, Mayer MA, Bock R, Baumann B, Liu JJ, Hornegger J, Fujimoto JG. Motion correction in optical coherence tomography volumes on a per A-scan basis using orthogonal scan patterns. Biomed Opt Express 2012; 3: 1182-1199.